NRIAG Journal of Astronomy and Geophysics (2017) 6, 162–173

National Research Institute of Astronomy and Geophysics

NRIAG Journal of Astronomy and Geophysics

www.elsevier.com/locate/nrjag

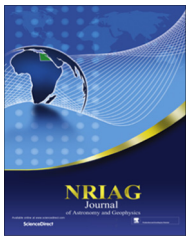

Relationships between electrical properties and petrography of El-Maghara sandstone formations, Egypt

Mohamed A. Kassab [a], **Mohamed M. Gomaa** [b,*], **Amir M.S. Lala** [c]

[a] *Exploration Dept., Egyptian Petroleum Research Institute, 11727 Cairo, Egypt*
[b] *Geophysical Sciences Dept., National Research Centre, Cairo, Egypt*
[c] *Geophysics Dept., Ain Shams University, Cairo, Egypt*

Received 5 October 2016; revised 9 January 2017; accepted 19 January 2017
Available online 9 February 2017

KEYWORDS

Conductivity;
Dielectric constant;
Frequency domain;
Jurassic;
Sandstone

Abstract Realization of electrical and petrography of rocks is absolutely necessary for geophysical investigations. The petrographical, petrophysical and electrical properties of sandstone rocks (El-Maghara Formation, North Sinai, Egypt) will be discussed in the present work. The goal of this paper was to highlight interrelations between electrical properties in terms of frequency (conductivity, permittivity and impedance) and petrography, as well as mineral composition. Electrical properties including (conductivity and dielectric constant) were measured at room temperature and humidity of (~35%). The frequency range used will be from 10 Hz to 100 kHz. Slight changes between samples in electrical properties were found to result from changes in composition and texture. Electrical properties generally change with grain size, shape, sorting, mineralogy and mineral composition. The dielectric constant decreases with frequency and increases with increasing clay content. The conductivity increases with the increase in conductor channels among electrodes. Many parameters can combine together to lead to the same electrical properties. The samples are mainly composed of sand with clay and carbonate.

1. Introduction and geologic setting

The elements of the samples will be separated electrically into semiconductor or nonconductor elements. Fig. 1 shows the location map of the samples.

El-Maghara section has a thickness of nearly 1900 m. It was subdivided into six marine and continental formations (Fig. 2, El Far, 1966; Kassab, 2004; Gomaa et al., 2015; Kassab et al., 2016). Samples are collected from Safa, Shusha and Mashaba

* Corresponding author.
E-mail address: mmmsgomaa@yahoo.com (M.M. Gomaa).
Peer review under responsibility of National Research Institute of Astronomy and Geophysics.

http://dx.doi.org/10.1016/j.nrjag.2017.01.002

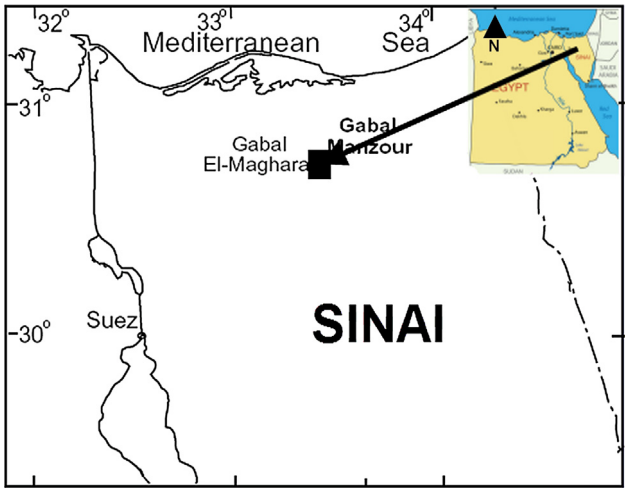

Fig. 1 Location map of the study area.

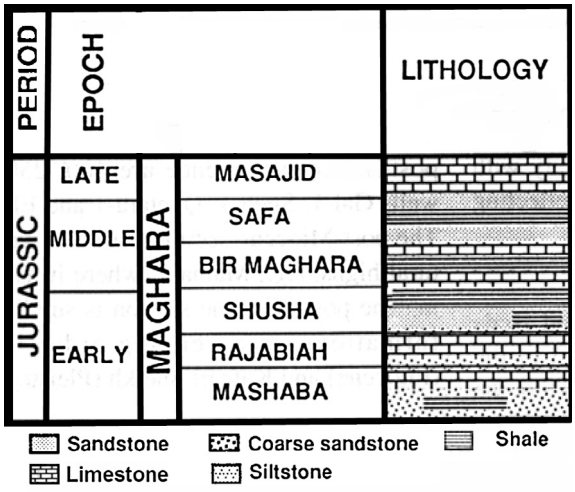

Fig. 2 A generalized stratigraphic column of Gebel El-Maghara in the northern Sinai area.

Formations. These three formations (from base to top) mostly consist of clastic rock samples (9 samples).

Geologic description of sampled formations is summarized as follows:

1- *Mashaba formation (bottom)*

It is the oldest Jurassic outcrop (thickness 100 m). It is composed of clay and sand, interbedded with shales and thin bed of sandy limestone, fine to coarse grained, overlain by thick sand bodies. The top part consists of clayey limestone and thin beds of sandstone.

2- *Shusha formation (middle)*

Some outcrops are detected at Shushat El-Maghara area (272 m thickness). The Shusha is formed from a clastic sequence interbedded with carbonate. The sediments consist of sand with some interbeds of shale and claystone which is the dominate part in the Formation. The top part is represented by argillaceous limestone.

3- *Safa formation (top)*

It is composed of sand and clayey sand with interbeds of limestone and clay in addition to some coal bearing facies (thickness of approximately 215 m).

The following is the description of the clastic rock samples collected from of the three formations (Mashaba, Shusha and Safa) according to the field observation.

2. Sample description

The following is the description of the clastic rock samples which are collected from the three formations (Mashaba, Shusha and Safa) according to field observation:

Sample M1 is ferruginous calcareous sandstone: Varicolored (dark brown and pale yellow), fine grained and hard, Mashaba Fm. Sample M15 is ferruginous clayey calcareous sandstone: Brownish white, fine to medium grained and hard, Mashaba Fm. Sample M32 is Sandstone: Light yellow with brown points, fine to medium grained and semi-hard, Shusha Fm. Sample M35 is ferruginous clayey calcareous sandstone: Light brown, very fine grained and hard, Shusha Fm. Sample M40 is ferruginous sandstone: Varicolor (pale white to yellow and brown), fine grained and semi-hard, Shusha Fm. Sample M47 is ferruginous sandstone: Brown, fine grained and hard, Shusha Fm. Sample M54 is sandstone: Pale yellow to light browns, fine grained and hard, Shusha Fm. Sample M71 is sandstone: Brown, fine grained and semi-hard, Safa Fm. Sample M87, Ferruginous Clayey Calcareous Sandstone: Pale red, fine grained and hard, Safa Fm.

3. Methodology

3.1. Petrography

Polarizing microscope was used to study thin sections for petrographical and mineralogical investigations. Impregnated blue dye was used to describe the sample pore spaces (Dickson, 1965). Fig. 3 represents the petrography photomicrographs and Fig. 4 represents the photomicrographs taken from Scanning Electron Microscope (SEM Model Philips XL 30 was used).

The samples were cleaned in the warm solvent extracted in extractor apparatus (soxhlets). Methanol and toluene were used as organic solvents for sample cleaning. The toluene removes any residual hydrocarbons (in pores) and the methanol removes water and salts from pores. At the end of this series, samples were dried at 90 °C until their weights were stable.

3.2. Petrophysics and electrical measurements

Porosity was measured using both matrix-cup helium porosimeter (gas-expansion method) and DEB-200 instrument (Archimedes' principle). Porosity ϕ is the proportion of the measured volume of pore space or void V_p (cm^3) to the total sample volume V_b (cm^3)

$$\phi = \frac{V_p}{V_b} \quad (1)$$

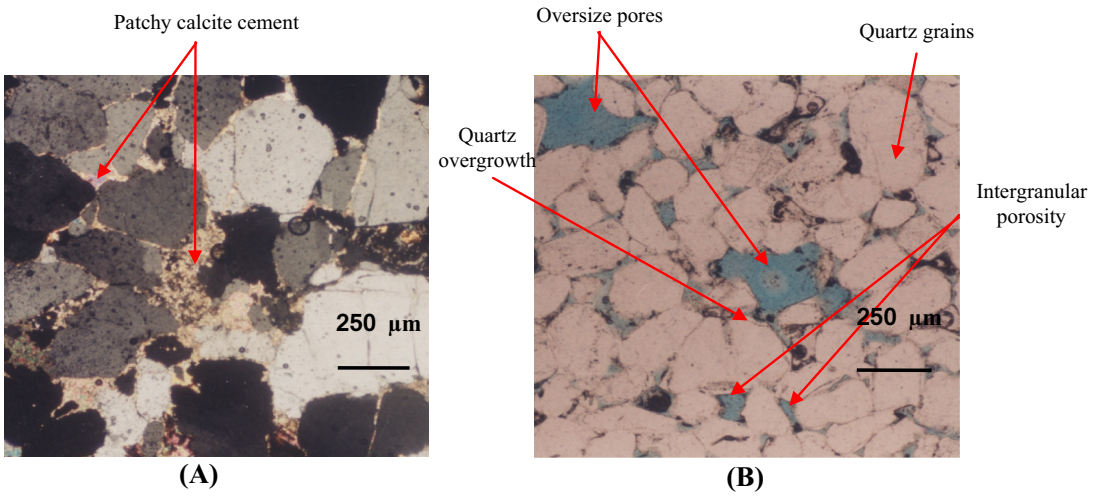

Fig. 3 Petrography photomicrographs.

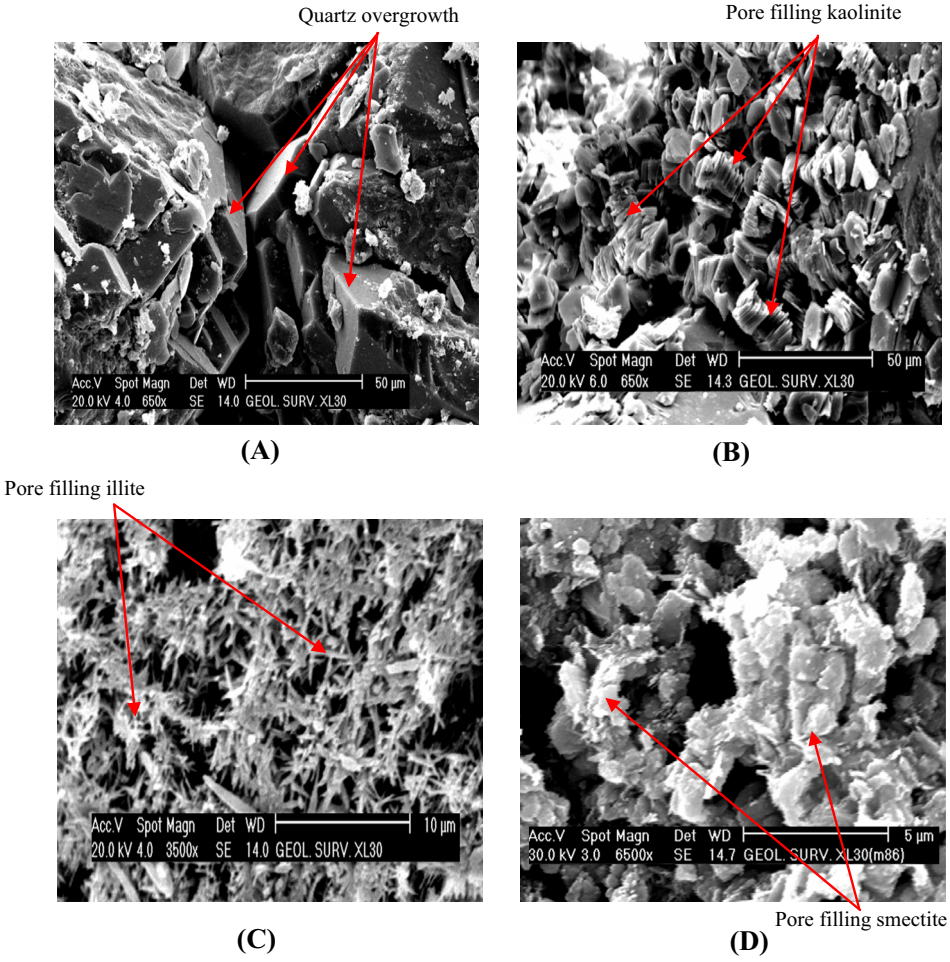

Fig. 4 SEM photomicrograph.

Bulk density (σ_b, g/cm^3) was calculated as follows:

$$\sigma_b = W_d / V_b \tag{2}$$

where W_d is dry sample weight (g). Grain density σ_g (g/cm^3) is as follows:

$$\sigma_g = W_d / V_g \tag{3}$$

where V_g is the grains volume (cm^3):

$$V_g = V_b - V_p \tag{4}$$

Gas permeability (K, in milli Darcy) was measured using gas permeameter supplied with nitrogen gas:

$$K = Q\mu L/(A\Delta P) \tag{5}$$

with Q is the rate of flow (cm^3/sec), μ is the fluid viscosity (centipoises), ΔP (atm./cm) is the pressure gradient, A is the cross-sectional area (cm^2) of the sample and L is its length (cm). The measured petrophysical factors are displayed in Table 1. In measuring permeability of rock samples by gas flow it is therefore necessary to make a correction for the type of gas and mean pressure. The measured permeability of a porous material to a gas is greater than that to a liquid. Klinkenberg correction must be applied to gas permeability, if we use these data for hydrocarbons production, to convert gas permeability into liquid permeability. But actual liquid or brine permeability is better than Klinkenberg due to fluid interaction with rock, especially in the presence of clay minerals. In our study we use the gas permeability for petrophysical facies only, so Klinkenberg correction was not applied to gas permeability.

For electrical measurements, the thickness and area of samples were prepared to be at least 1:5 to avoid stray capacitance. The specimen faces were adjusted to have parallel faces. All Jurassic ages are represented in the measured specimens. Hioki 3522- 50 LCR instrument was used in the frequency range from 10 Hz up to 100 kHz (nearly 10 frequencies in each decade) with the help of non-polarizing electrodes ($Cu/CuSO_4$) (Gomaa, 2009; Shaltout et al., 2012).

Electrical properties were measured in parallel arrangement. Measured parameters were parallel capacitance (C_p) and parallel conductance (G_p). The complex relative permittivity ε^* can be written as

$$\varepsilon^* = \varepsilon' - i\varepsilon'' \tag{6}$$

where measured relative permittivity (ε') before correction is

$$\varepsilon' = \frac{C_p d}{\varepsilon_0 A} \tag{7}$$

and the imaginary part of the relative dielectric constant (ε'') is

$$\varepsilon'' = \frac{G_p d}{\omega \varepsilon_0 A} \tag{8}$$

A is the sample cross-sectional area, d is the thickness of sample, ε_0 is the permittivity of free space (8.85×10^{-12} F/m), and ω is the angular frequency. The real part of conductivity is equal:

$$\sigma' = G_p \frac{d}{A} = \varepsilon'' \omega \varepsilon_0 \tag{9}$$

Samples are measured dry. The complex series impedance (Z)

$$Z = R_s - iX_s \tag{10}$$

where R_s is the series resistance and X_s is the reactance

Measurements were made at humidity of (35%) and room temperature (27 °C) in an isolated chamber.

Fringing errors (of capacitance) are included using (Chew and Kong, 1980; Gomaa and Alikaj, 2010) formula

$$C \approx \frac{a^2 \pi \varepsilon_r \varepsilon_0}{d}\left\{1 + \frac{2d}{\pi \varepsilon_r a}\left[\ln\left(\frac{a}{2d}\right) + (1.4\varepsilon_r + 1.8) + \frac{d}{a}(0.27\varepsilon_r + 1.7)\right]\right\} \tag{11}$$

where a is the sample radius and ε_r is the relative dielectric constant.

The electrode resistance is very small at the entire frequency domain and it was removed from measurements (as was discussed in Gomaa, 2008, 2013).

4. Results and discussion

4.1. Petrography

4.1.1. Microfacies analyses

The studied El Maghara sandstones samples can be subdivided into two microfacies: quartz arenite and calcareous quartz arenite microfacies.

Quartz arenite microfacies: Some parts are represented by Quartz arenite microfacies which are composed of moderately sorted, fine to medium, subrounded to subangular quartz grains cemented together by silica cement and iron oxides which reduce slightly the pore spaces between grains (Fig. 3B). It is composed of quartz grains (99.7%) in addition to carbonate that is mostly represented by calcite (7.3%) and slightly of silt and claystone (4.6%). Quartz grains are mainly monocrystalline which are compacted together through suture and concave-convex contact with slight effect on the total pore volume. Few ferruginated clay patches are present. Porosity of the quartz arenite samples is mostly poor to excellent values (1.61–18.52%), represented by intergranular pore spaces in addition to oversize pores, due to the dissolution of some quartz grains (Fig. 3B).

Calcareous quartz arenite microfacies: These microfacies represent most of the parts of El Maghara sandstone formations. It is composed of ill sorted, fine to coarse quartz grains (77.6%) in addition to some carbonate mostly represented by

Table 1 Petrophysical parameters of sandstone samples.

Sample no.	Porosity %, (Helium)	Bulk density, g/cm^3	Grain density, g/cm^3	Permeability, mD	Silt & Clay %	Sand %	Carbonate %	Formation
M1	3.47	2.57	2.65	0.94	5.3	77.6	17.1	Mashaba
M15	3.34	2.57	2.66	0.069	8.1	60.7	31.2	Mashaba
M32	15.13	2.21	2.61	944.55	0.3	99.7	0	Shusha
M35	4.63	2.58	2.71	0.067	10.5	66	23.5	Shusha
M40	11.57	2.30	2.61	67.31	4.6	88.1	7.3	Shusha
M47	1.61	2.58	2.62	1.22	4.5	91.6	3.9	Shusha
M54	0.43	2.74	2.72	1.321	6.9	57.8	35.3	Shusha
M71	18.52	2.11	2.59	1158.66	2.7	93.2	4.1	Safa
M87	1.07	2.59	2.61	0.097	6.6	55.1	38.3	Safa

calcite (38.3%), silt and claystone (2.74%) and some bioclastic remains (Fig. 3A). Quartz grains are mainly monocrystalline that is compacted together through suture and concave-convex contact with slight effect on the total pore volume, where the grains are mostly floating within the cement. Grains are cemented by carbonate cement mostly (calcite). In addition to calcite, some ferruginated clay patches are present, which highly reduce the pore spaces. These microfacies are mostly characterized by poor porosity values (0.43–4.63%). The pore porosity is represented by intergranular pore spaces which are highly reduced by calcite and micro fractures porosity, due to stress acted on grains (Fig. 3A).

4.1.2. Effect of diagenesis on the pore volume

Petrographical examination of the studied samples reveals that they are mainly Quartz Arenite. Fig. 3 shows the petrography photomicrographs and Fig. 4 shows SEM photomicrographs. Grains are poorly sorted, fine to coarse, subrounded to subangular, and cemented together by slightly iron oxides and silica cement (Fig. 3B) or by calcite cement (Fig. 3A). The diagenetic processes have a great effect on the petrophysical properties of sedimentary rocks as they reduce and/or enhance the porosity of samples. Dissolution, leaching out of some quartz grains (Fig. 3B) leads to increase the porosity. Compaction processes (Fig. 3A and B), cementation by silica cement (Fig. 3B and Fig. 4A), iron oxides and calcite cement (Fig. 3A) and formation of authigenic minerals reduce porosity, where the interstitial pore spaces are mainly filled with clay minerals, leading to reduce porosity (Fig. 4B–D). Kaolinite is the most dominant clay mineral (Fig. 4B). Also, Illite (Fig. 4C) and Smectite (Fig. 4D) are detected in the studied samples. The leaching is represented by the presence of high porosity after the dissolving of silicate minerals (Fig. 3B). Porosity is represented mainly by intergranular porosity (Fig. 3B).

4.2. Petrophysical properties

Based on the petrophysical behavior, the obtained data for sandstone samples refer to that the bulk density σ_b values are the contribution of both grain and pore phases. The bulk density is mostly dependent on porosity ϕ with highly reliable relationship ($R^2 = -0.96$, Fig. 5). Bulk density is calculated using the following:

$$\phi = 83.94 - 31.28\sigma_b \quad (R^2 = -0.96) \tag{12}$$

The permeability (k) for the studied samples is mostly ranked as poor to excellent values reaching up to 1158 mD in average. Fig. 6 shows the permeability values plotted against the porosity measured using helium. It is mostly dependent on porosity with more reliable relationship with porosity. The regression equation calculated for these relations is as follows:

$$k = 0.1022e^{0.5248\phi} \quad (R^2 = 0.81) \tag{13}$$

4.3. Electrical properties

The frequency response of the electrical properties is dominated by low frequency dispersion. The variation of AC electrical properties has been investigated and evaluated in the frequency range of 10 Hz–100 kHz (room temperature). Fig. 7 represents the relative permittivity against frequency.

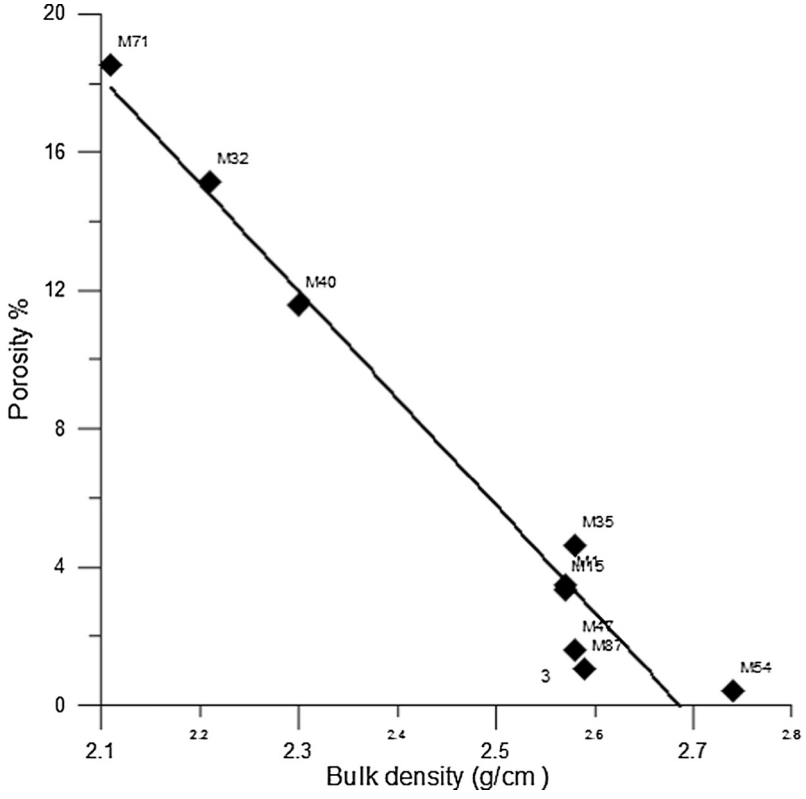

Fig. 5 Porosity – bulk density relationship.

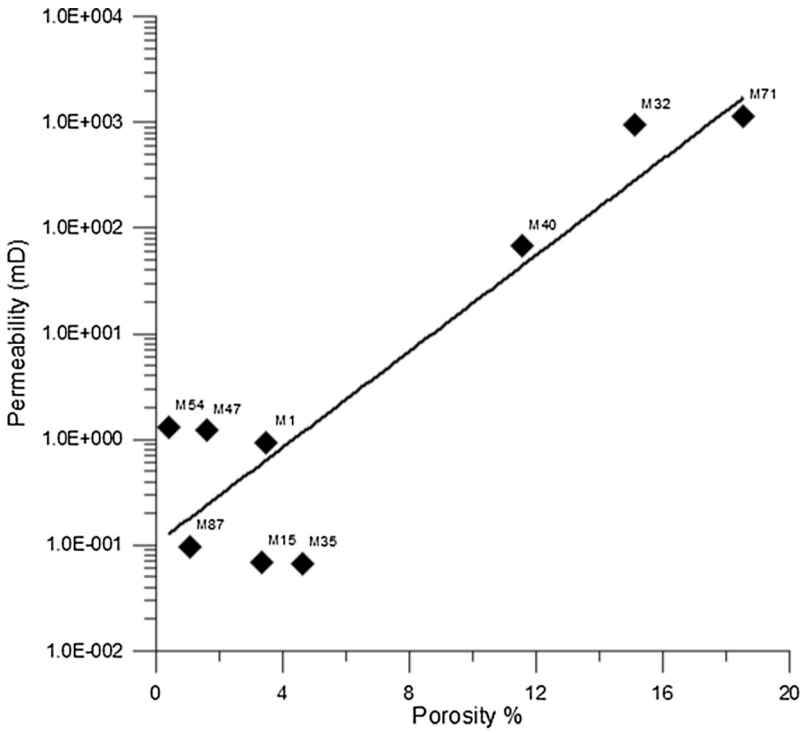

Fig. 6 Permeability - porosity relationship.

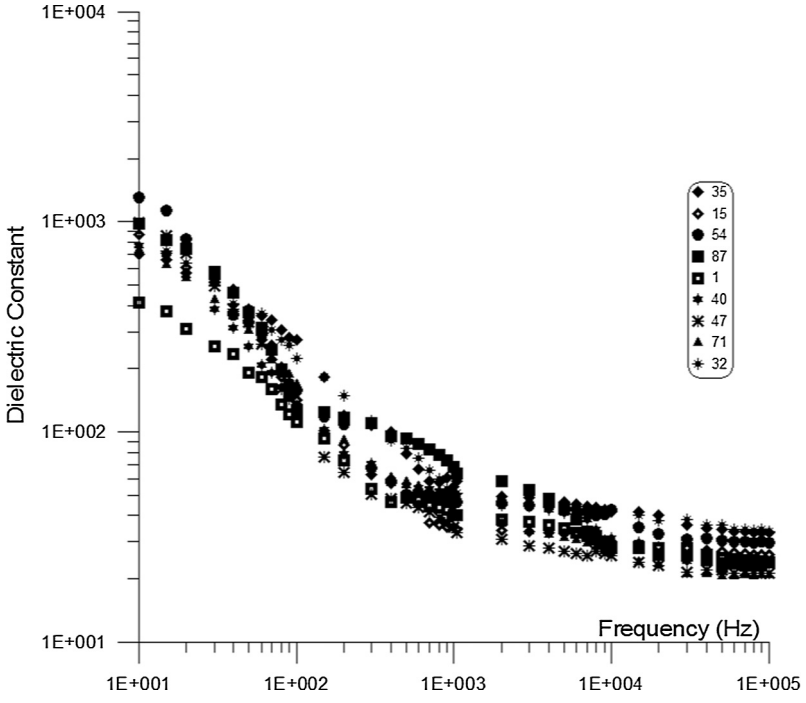

Fig. 7 The dielectric constant versus frequency for sandstone samples.

Values of dielectric constant (ε'), at high frequencies, are nearly frequency independent and decrease with increasing frequency, due to polarization. Values of relative permittivity decrease with frequency increase, and then achieve a steady value because beyond a certain frequency and the hopping of electrons cannot follow the applied alternating field (Chelidze and Gueguen, 1999), i.e. the speed of the electrons cannot follow the speed of the applied field. The progressive decrease in relative permittivity with decrease in the whole concentration of conductor is the result of the increase in void distances between grains, i.e. increasing the pore spaces between the conducting solid phases. The capacitance progressively increases

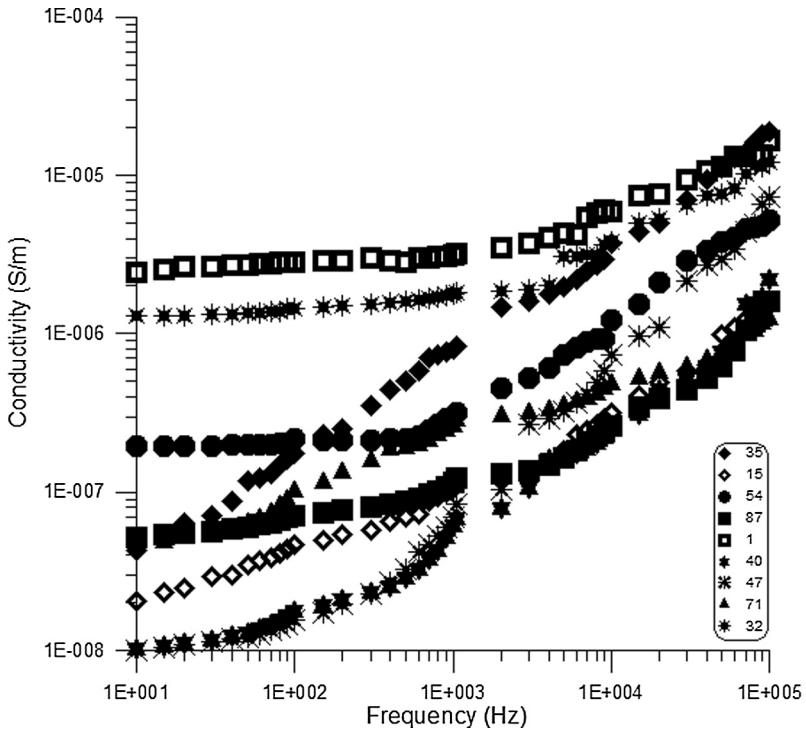

Fig. 8 The conductivity versus frequency for sandstone samples.

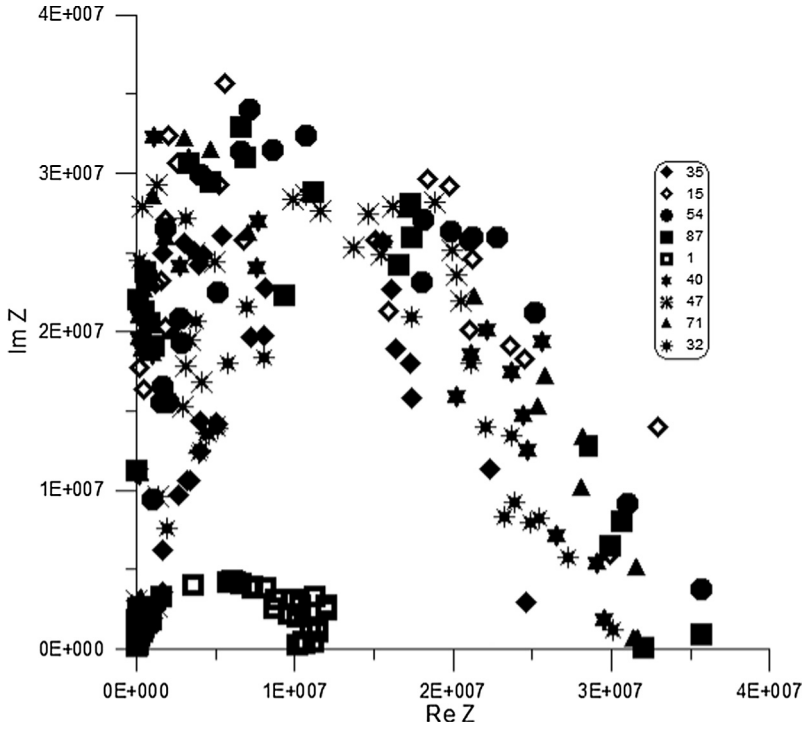

Fig. 9 The impedance plane of sandstone samples.

with frequency decrease or with the whole conductor concentration increase (Chelidze et al., 1999). The variation with frequency in ε' can be attributed to Maxwell–Wagner polarization, i.e. the heterogeneity in rocks leads to a frequency dependence of the dielectric constant. Heterogeneity motivates charge transports to be collected at conducting grain edges and produces the interfacial polarization. Variation of relative dielectric constant with frequency for all samples has demonstrated nearly similar behavior, indicating that they follow the same power law (Jonscher, 1999). Additionally,

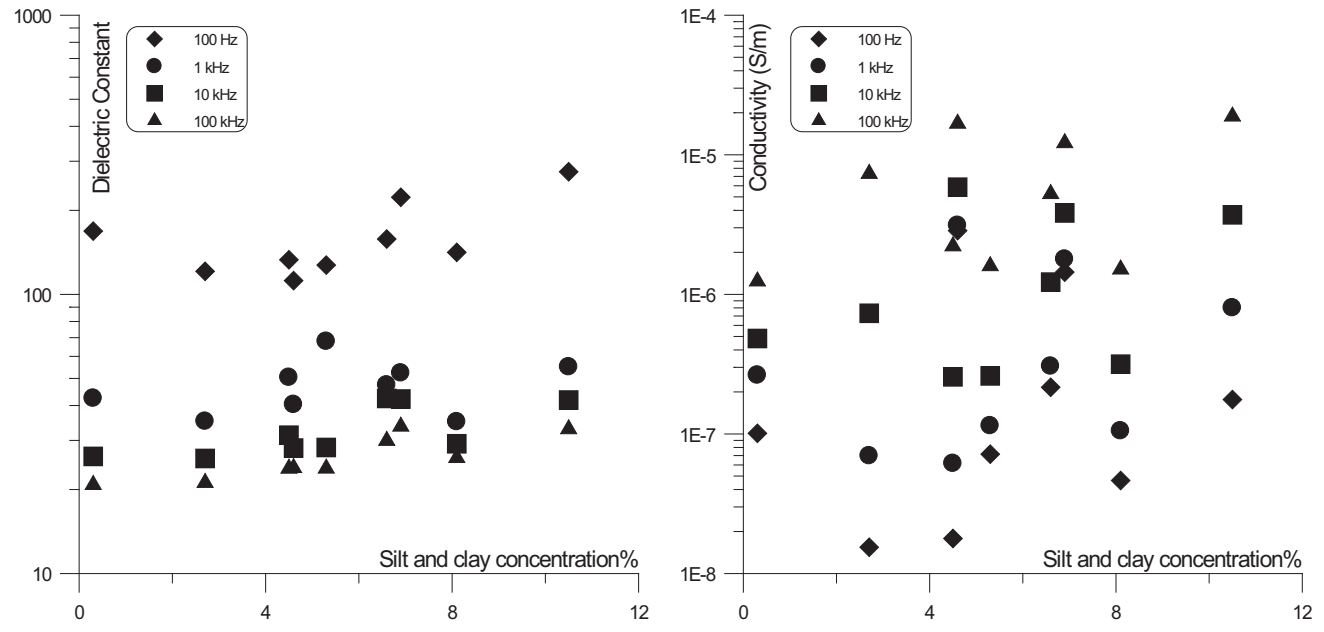

Fig. 10 The dielectric constant and conductivity versus silt and clay concentration (%) of sandstone samples.

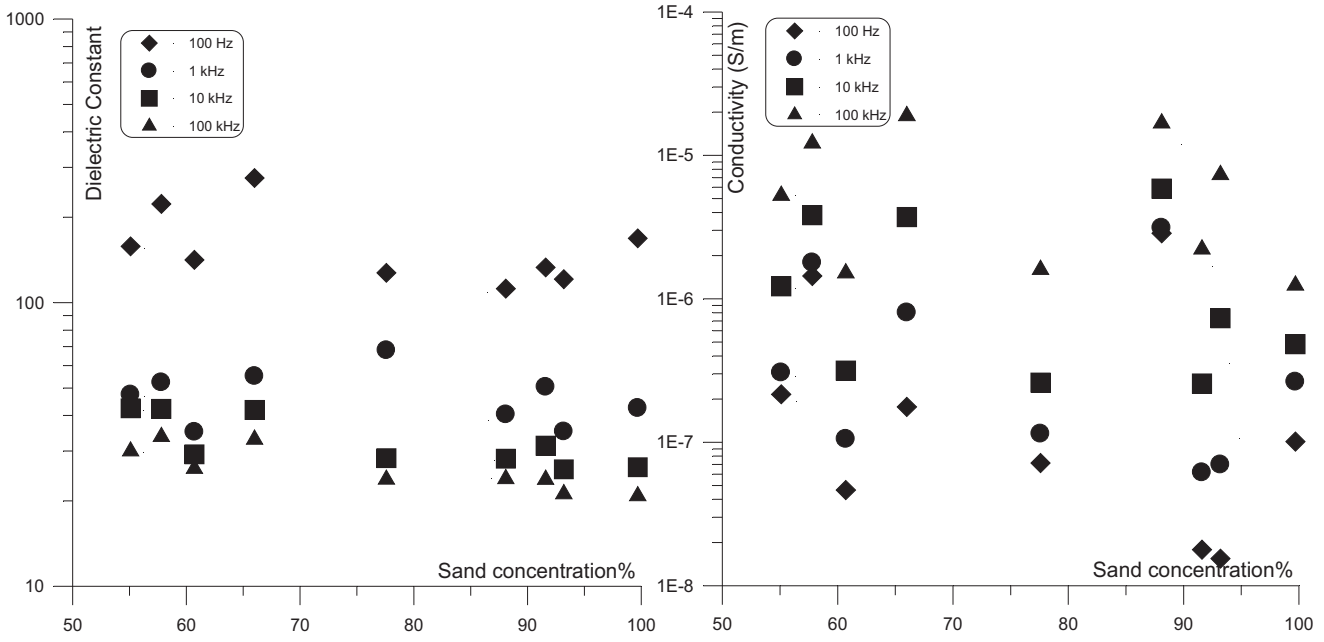

Fig. 11 The dielectric constant and conductivity versus sand concentration (%) of sandstone samples.

the behavior of dielectric constant dispersion is related to the application of a field that serves for the hopping of electrons between two different sites in the atoms. This one also leads to an increase in the electronic component support to dielectric constant variation. At high frequencies, the charge carriers could not follow the rotation of the electric field, so their fluctuation or rotation will begin to delay behind the applied field leading to a decrease in dielectric constant. Sample (M54) has the highest value of relative permittivity (lowest porosity), while sample (M1) has the lowest value (Fig. 7) (may be due to texture).

Fig. 8 shows the conductivity versus frequency for all samples. Conductivity, generally, increases with frequency increase and with total conductor concentration (Levitskaya and Sternberg, 1996a, 1996b). The general increase in conductivity is not ordered due to the randomness and heterogeneity in the samples. There is only one slope with frequency for some samples (samples 15 and 35) and there are two slopes with frequency for the other samples (texture effect). At relatively low frequencies, the conductivity is low and nearly flat (for samples of two slopes). The increase in conductivity at higher frequencies is due to the formation of more continuous

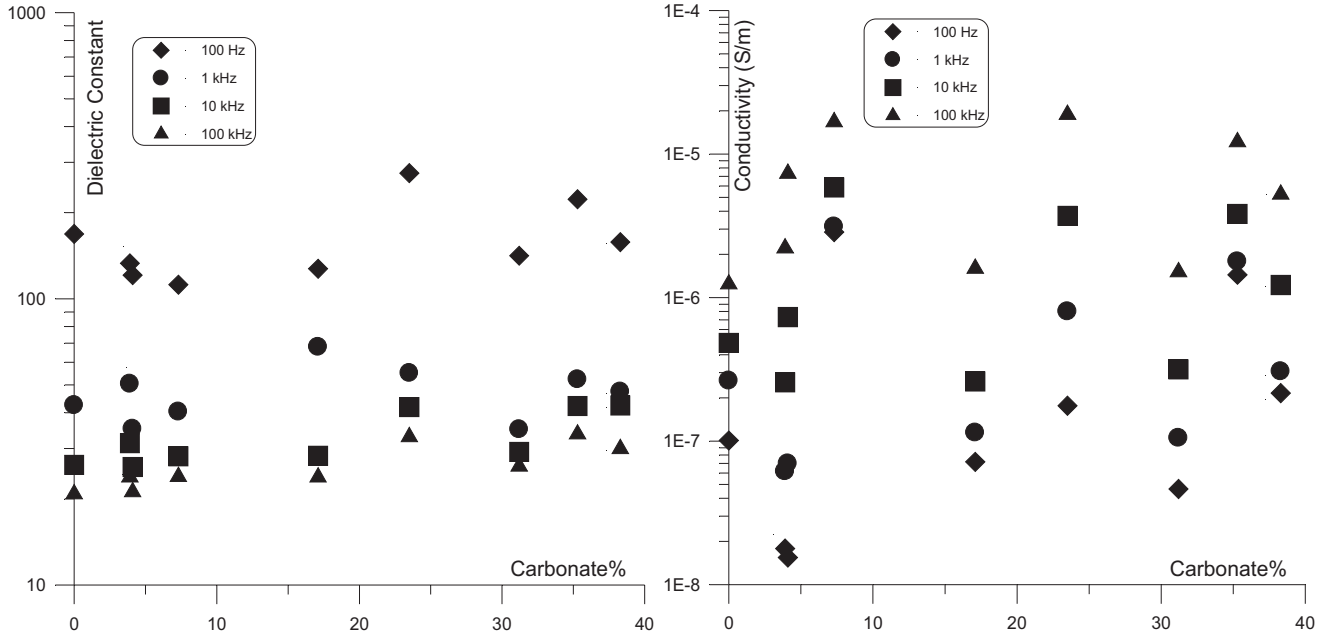

Fig. 12 The dielectric constant and conductivity versus carbonate concentration (%) of sandstone samples.

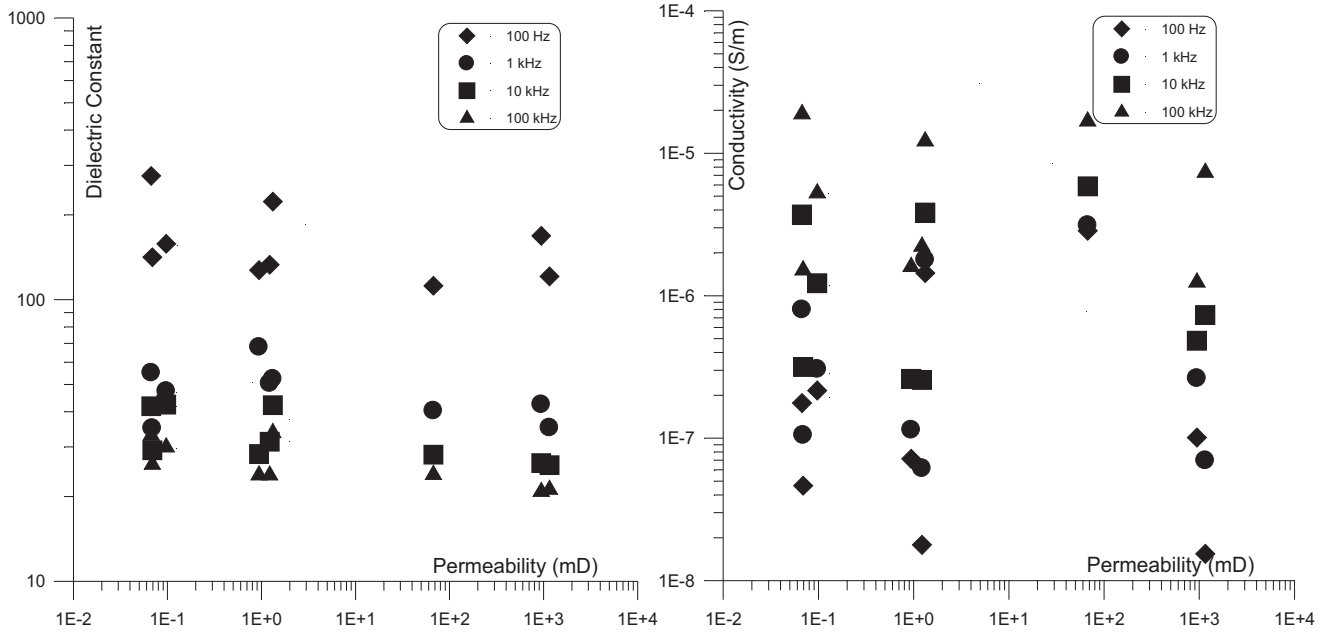

Fig. 13 The dielectric constant and conductivity versus permeability of sandstone samples.

conduction paths (Knight, 1983; Levitskaya and Sternberg, 2000). With the increase in frequency particles are motivated to overcome the energy level barriers to form continuous conduction channels and as a result of that the conductivity increases (Jonscher, 1999; Gomaa and Elsayed, 2009; Gomaa et al., 2009). Concentration of conductor (mud) increases the efficiency of the conductor continuous paths and as a result increases the experimental conductivity. The conductivity behavior shows power law (nearly) with frequency (ω),

$$\sigma \propto \omega^n \tag{14}$$

where n is the curve slope ($\sim$0.63 to $\sim$0.43) for samples of one slope. The low frequency slope may be the result of DC conduction (conducting elements). The samples of high conductivity values are M1, M32 and M54, whereas those with low values of conductivity are M40, M47 and M15 (Fig. 8).

The frequency dependence of conductivity is a function of polarization effects. An analogy between specimens and electrical equivalent circuit is done by supposing a capacitance

between conductor grains. When conductor grain concentration is high, then conductivity is determined essentially from the conducting links. Up to a certain frequency, the conductivity of the samples will not change significantly. Above that frequency the capacitor contribution (insulator grains) is very huge. Near percolation threshold P_C, few conducting grain links may be found and the air gab (capacitors) effect among conductor grains begins to be very huge (Efros and Shklovskii, 1976). With the increase in frequency, the current in gabs (capacitors) increases and the final result of the whole conductivity will be increased (Song et al., 1986).

The diffusion within clusters contributes to conductivity frequency dependence (above P_C) and the polarization effects between semiconducting grains (Knight, 1983; Knight and Endres, 1990). Within frequency range, the conductivity has a flat response for most of the samples. This is because electrons are free to move over large distances under electric field. For highly conducting samples (M1, M32 and M54), electrons can move through many and different paths in the infinite clusters. Near critical concentration only a few percolating paths are present and movement of electrons in the finite paths is of great significance and conduction mechanism will increase with frequency.

Below P_C region, the polarization and the movement of electrons in the conducting paths will define conductivity values. Finally, conductivity will increase with frequency increase. Sample below the percolation region P_C will follow the formula $\sigma \propto \omega^2$.

The energy dissipated at low frequencies is due to the polarization between isolated conducting grains. Near P_C there is a consistent transformation from ω^n to ω^2 behavior (Levitskaya and Sternberg, 1996a, 1996b; Levitskaya and Sternberg, 2000). However, even for samples near percolation threshold P_C (Fig. 8) the asymptotic ω^2 is not present (> 100 Hz).

Fig. 9 displays complex impedance representation. Generally, low conductor from mud is represented by a line in the impedance plot. That arc decreases in size (part of semicircle) at high conductor concentrations (Ruffet et al., 1991a, 1991b). Samples M71 and M47 show an arc, while samples M54, M87, M40 and M32 show a semicircle. The distances between conducting grains decrease with conductor increase, until percolation threshold, and then the characteristic appearance of the curve changes from a line to an arc and then to a semicircle.

Fig. 10 shows measurements of experimental conductivity and dielectric constant values versus mud concentration percentage at different frequencies (100 Hz, 1, 10 and 100 kHz), respectively. Increase in mud concentration, increases the dielectric constant because insulating distances between conducting grains decrease. These distances between conducting grains decrease up to the first continuous conductor channel is formed. At high frequency (100 kHz) the dielectric constant shows a value from 20 to 200. The total conductor concentration (mud) in the samples does not reach the critical concentration. With the increase in mud the continuous channels of conductor grains between electrodes increase at the expense of insulator paths and accordingly the conductivity increases.

Fig. 11 shows the conductivity and dielectric constant versus sand concentration percentage at different frequencies (100 Hz, 1, 10 and 100 kHz). Dielectric constant, generally, does not change with increasing sand in sample because the distances between conducting grains do not reach critical concentration and not also near it (Gomaa and Kassab, 2016). The distances between conducting grains are very big to show a difference in dielectric constant. The conductivity shows a general increase within one decade followed by a general decrease due to the general differences between samples in homogeneity and texture.

Fig. 12 shows the conductivity and dielectric constant versus carbonate concentration percentage at different frequencies (100 Hz, 1, 10 and 100 kHz). The same can be

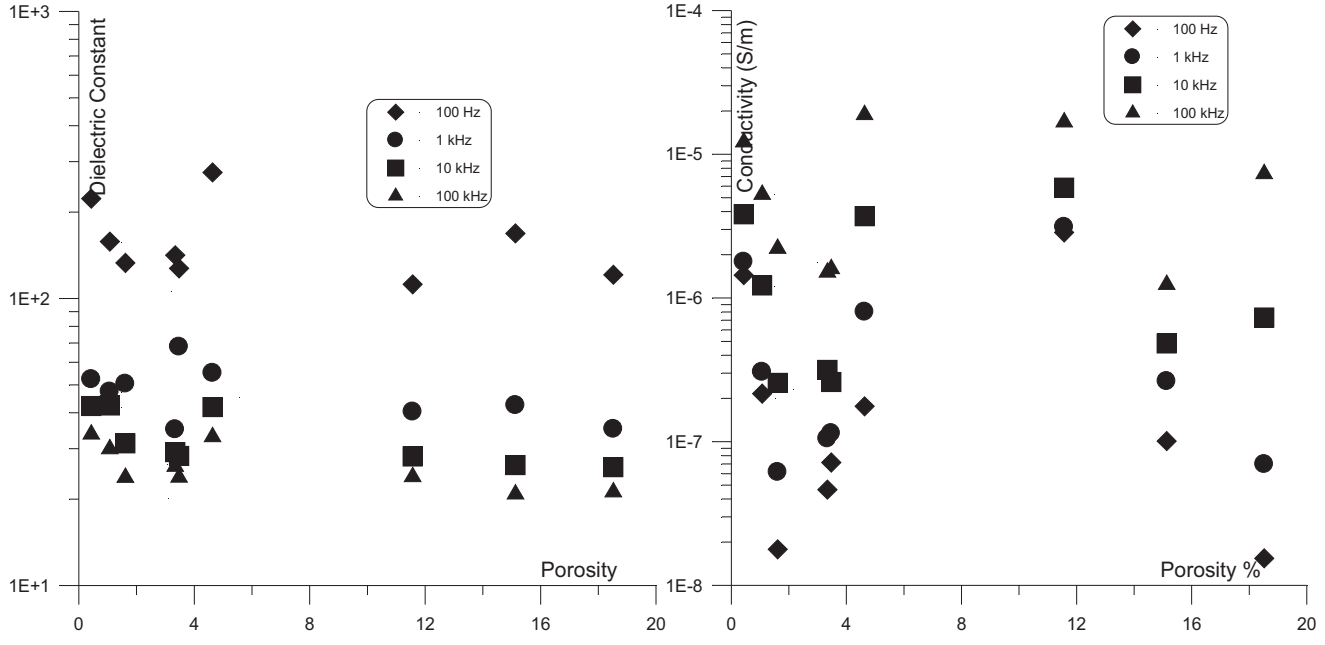

Fig. 14 The dielectric constant and conductivity versus porosity (%) of sandstone samples.

seen in Fig. 11 for dielectric constant and conductivity. This may be due to the fact that the sand and clay are relatively insulators with different conductivities (Gomaa and Kassab, 2016).

Fig. 13 shows the conductivity and dielectric constant with permeability at different frequencies (100 Hz, 1, 10 and 100 kHz). There is a common slight decrease in dielectric constant with permeability increase at low frequency, while the decrease is less for higher frequencies. This relation is not clear enough (sample number is not enough). The conductivity displays a flat response against the permeability.

Fig. 14 shows the conductivity and dielectric constant versus porosity for samples at different frequencies (100 Hz, 1, 10 and 100 kHz). There is a common slight decrease in the relative dielectric constant with porosity increase at low frequencies and tends to be stable for higher frequencies. The conductivity shows a general increase followed by a general porosity.

The arrangement and relations between the grains or elements in samples are very great and may be changed at the same sample (Sen, 1981; Olhoeft, 1985) even if they have the same concentration and combination of materials (Abou El-Anwar and Gomaa, 2013).

5. Conclusions

The paper purpose was to highlight on arrangement and relations between the grains and their relation to electrical properties as a function of frequency (conductivity, permittivity and impedance). Also, the relation between mineral composition and petrography was discussed. Based on the mineralogical composition, the Jurassic sandstones of El Maghara area are mainly quartz arenite. Most samples have high porosity. Origin of porosity in most of the samples is primary (intergranular porosity) and few samples have secondary (oversize pores) porosity. Porosity is controlled by diagenetic processes (cementation, compaction and formation of authigenic minerals), which greatly reduces the pore spaces. Other diagenetic processes may lead to enhancing porosity (dissolution and leaching). The sandstone rocks are characterized by relatively good porosity and permeability, and these sandstones can be considered as a good reservoir rocks.

The frequency range measurement of electrical properties was from 10 Hz up to 100 kHz. The minor fluctuations in electrical measurements may be due to the fluctuations in arrangements and relations between the grains or elements in samples. Enhancement of dielectric constant is referred to increase in clay concentration. All samples are supposed to be below the critical concentration of the mud. Many parameters can join together to give the same electrical properties. Increase in conductivity is referred to the increase in conduction arrangements and relations between electrodes. There are many controlling factors on electrical properties.

References

Abou El-Anwar, E., Gomaa, M.M., 2013. Electrical properties and geochemistry of carbonate rocks from the Qasr El-Sagha formation, El-Faiyum, Egypt. Geophys. Prospect. 61, 630–644.

Chelidze, T., Gueguen, Y., 1999. Electrical spectroscopy of porous rocks: a review-I. Theoretical models. Geophys. J. Int. 137, 1–15.

Chelidze, T., Gueguen, Y., Ruffet, C., 1999. Electrical spectroscopy of porous rocks: a review-II. Experimental results and interpretation. Geophys. J. Int. 137, 16–34.

Chew, W.C., Kong, J.A., 1980. Effects of fringing fields on the capacitance of circular microstrip disk. IEEE Trans. Microw. Theory Tech. MTT-28 (2), 98–104.

Dickson, J.A.D., 1965. A modified staining technique for carbonates thin-section. Nature 205, 587.

Efros, A.L., Shklovskii, B.I., 1976. Critical behavior of conductivity and dielectric constant near the metal–non-metal transition threshold. Phys. Status Sol. 76, 475–489.

El Far, D.M., 1966, Geology and coal deposits of Gebel El-Maghara (Northern Sinai), Geol. Sury. and Min. Res. Depart. Cairo, Egypt, Paper No. 37, p. 59.

Gomaa, M.M., 2008. Relation between electric properties and water saturation for hematitic sandstone with frequency. Ann. Geophys. 51 (5/6), 801–811.

Gomaa, M.M., 2009. Saturation effect on electrical properties of hematitic sandstone in the audio frequency range using non-polarizing electrodes. Geophys. Prospect. 57, 1091–1100.

Gomaa, M.M., 2013. Forward and inverse modeling of the electrical properties of magnetite intruded by magma, Egypt. Geophys. J. Int. 194 (3), 1527–1540.

Gomaa, M.M., Alikaj, P., 2010. Effect of electrode contact impedance on a. c. electrical properties of wet hematite sample. Mar. Geophys. Res. 30 (4), 265–276. http://dx.doi.org/10.1007/s11001-010-9092-y.

Gomaa, M.M., Elsayed, M., 2009. Thermal effect of magma intrusion on electrical properties of magnetic rocks from Hamamat Sediments, NE Desert, Egypt. Geophys. Prospect. 57 (1), 141–149.

Gomaa, M.M., Kassab, M., 2016. Pseudo random renormalization group forward and inverse modeling of the electrical properties of some carbonate rocks. J. Appl. Geophys. 135, 144–154.

Gomaa, M.M., Shaltout, A., Boshta, M., 2009. Electrical properties and mineralogical investigation of Egyptian iron ore deposits. Mater. Chem. Phys. 114 (1), 313–318.

Gomaa, M.M., Kassab, M.A., El–Sayed N, A., 2015. Study of pertrographical and electrical properties of some Jurassic carbonate rocks, north Sinai, Egypt. Egypt. J. Petrol. 24, 343–352.

Jonscher, A., 1999. Dielectric relaxation in solids. J. Phys. D: Appl. Phys. 32, R57–R70.

Kassab, M., 2004. Petrophysical studies on Jurassic rocks in Gulf of Suez and North Sinai and its implementations for hydrocarbon exploration Ph. D. thesis. Ain Shams University, Cairo, Egypt.

Kassab, M.A., Abuseda, H.H., El Sayed, N.A., LaLa, A.M., Elnaggar, O.M., 2016. Petrographical and petrophysical integrated studies, Jurassic rock samples, North Sinai, Egypt. Arab. J. Geosci. 9 (99). http://dx.doi.org/10.1007/s12517-015-2146-3.

Knight, R.J., Endres, A.L., 1990. A new concept in modeling the dielectric response of sandstones: defining a wetted rock and bulk water system. Geophysics 55, 586–594.

Knight, R., 1983. The use of complex plane plots in studying the electrical response of rocks. J. Geomag. Geoelectr. 35, 767–776.

Levitskaya, M.T., Sternberg, K.B., 1996a. Polarization processes in rocks 1. Complex dielectric permittivity method. Radio Sci. 31 (4), 755–779.

Levitskaya, M.T., Sternberg, K.B., 1996b. Polarization processes in rocks 2. Complex dielectric permittivity method. Radio Sci. 31 (4), 781–802.

Levitskaya, T.M., Sternberg, B.K., 2000. Application of lumped-circuit method to studying soils at frequencies from 1 kHz to 1 GHz. Radio Sci. 35 (2), 371–383.

Olhoeft, G.R., 1985. Low frequency electrical properties. Geophysics 50, 2492–2503.

Ruffet, C., Guéguen, Y., Darot, M., 1991a. Rock conductivity and fractal nature of porosity. Terra Nova 137, 265–275.

Ruffet, C., Guéguen, Y., Darot, M., 1991b. Complex measurements and fractal nature of porosity. Geophysics 137, 758–768.

Sen, P.N., 1981. Dielectric anomaly in inhomogeneous materials with application to sedimentary rocks. Appl. Phys. Lett. 39 (8), 667–668.
Shaltout, A.A., Gomaa, M.M., Wahbe, M., 2012. Utilization of standard-less analysis algorithms using WDXRF and XRD for Egyptian Iron Ores identification. X-Ray Spectrom. 41, 355–362.
Song, Y., Noh, T.W., Lee, S., Gaines, R., 1986. Experimental study of the three- dimensional ac conductivity and dielectric constant of a conductor- insulator composite near the percolation threshold. Phys. Rev. B 33 (2), 904–908.